Electromagnetics
Publication details, including instructions for authors and subscription information:
http://www.tandfonline.com/loi/uemg20

Application of the Array Scanning Method in Periodic Structures with Large Periods

Ahmad Bakhtafrouz[a] & Amir Borji[b]
[a] Department of Electrical and Computer Engineering, Isfahan University of Technology, Isfahan, Iran
[b] Department of Electrical Engineering, Sharif University of Technology, Tehran, Iran
Published online: 22 Jun 2015.

Electromagnetics, 35:293–309, 2015

ISSN: 0272-6343 print/1532-527X online
DOI: 10.1080/02726343.2015.1047729

Taylor & Francis
Taylor & Francis Group

Application of the Array Scanning Method in Periodic Structures with Large Periods

AHMAD BAKHTAFROUZ[1] and AMIR BORJI[2]

[1]Department of Electrical and Computer Engineering, Isfahan University of Technology, Isfahan, Iran
[2]Department of Electrical Engineering, Sharif University of Technology, Tehran, Iran

Abstract *The problem of aperiodic excitation of periodic structures with periods larger than a half-wavelength is revisited. A large number of antennas and other electromagnetic wave propagation problems fall within this category. Because of overlapping branch cuts, the conventional path deformation techniques employed in application of the array scanning method for this type of problem fail when the period is larger than a half-wavelength. A new method based on the subdivision of the integration path and using the double exponential quadrature formula is introduced to alleviate this problem and apply the array scanning method to structures with an arbitrary spatial period. To demonstrate the application of the new method and to validate the results, reflection and transmission coefficients of a frequency selective surface excited by a single electric dipole are calculated. Near fields of the frequency selective surface with aperiodic excitation are obtained and compared with those of a commercial electromagnetic simulator. The proposed method, similar to the path deformation technique, which is applicable to small periods, shows considerable advantage in terms of computational time and memory requirement.*

Keywords aperiodic sources, array scanning method, double exponential quadrature rule, frequency selective surface, periodic structures

1. Introduction

Periodic structures have been used in a wide variety of optical, microwave, and antenna applications (Llombart et al., 2005; Lee et al., 2005; Zhao et al., 2005). Planar or 2D periodic structures can be divided into several main categories, including electromagnetic bandgap (EBG) structures, photonic crystals (PCs), artificial magnetic conductors (AMCs), and frequency selective surfaces (FSSs). EBGs and PCs are usually employed to suppress or slow down the propagation of electromagnetic waves in a certain range of frequencies (Llombart et al., 2005), while FSSs are usually used for spatial filtering (Lee et al., 2005). Periodic structures also form the basis of many leaky wave antennas (Zhao et al., 2005).

Received 15 July 2014; accepted 1 November 2014.
Address correspondence to Ahmad Bakhtafrouz, Department of Electrical and Computer Engineering, Isfahan University of Technology, Isfahan, 84156-83111, Iran. E-mail: bakhtafrouz@ec.iut.ac.ir
Color versions of one or more of the figures in the article can be found online at www.tandfonline.com/uemg

In analysis of periodic structures with planewave excitation, the Floquet periodicity of planewaves helps to reduce the problem to a unit cell and solve the resulting equations with a numerical method, such as the method of moments (MoM), finite element method (FEM), or finite difference time domain (FDTD), after applying the periodic boundary conditions (Yang & Rahmat-Samii, 2009). However, in many practical cases, the excitation is aperiodic, such as a single dipole; thus, the scattering problem is not a periodic one, and the above-mentioned analysis is not applicable anymore (Araneo et al., 2011; Lovat et al., 2011; Capolino et al., 2005a, 2005b; Rodriguez-Berral et al., 2009; Yang, 1999, 2001, 2004). For these cases, two methods have been employed: the planewave expansion method (PWM) and the array scanning method (ASM). In Capolino et al. (2007), both methods were thoroughly explained, and it was shown that the ASM had a superior performance because of the finite interval of spectral integration involved.

The ASM was used in the analysis of phased array antennas in Munk and Burrell (1979). Recently, the ASM has been applied to analyze a number of periodic structures excited with a finite aperiodic source. Analysis of periodic microstrip lines excited by a delta-gap source (Rodriguez-Berral et al., 2009), antenna radiation from photonic bandgap materials (Yang, 1999), analysis of PC slabs excited by a microstrip dipole or a line source (Yang, 2004), mode excitation of EBG waveguides (Capolino et al., 2005b), shielding effectiveness of periodic screens (Araneo et al., 2011), and dipole excitation of periodic screens (Lovat et al., 2011) are just a few examples of using ASM.

Evaluation of near fields for a dipole excited periodic structure after solving the integral equation (IE) and using the ASM can only be found in Lovat et al. (2011). However, in this work, all examples have spatial periods less than a half-wavelength, and the path deformation technique has been successfully used. As noted in Lovat et al. (2011) and Capolino et al. (2007), in periodic structures with periods larger than a half-wavelength, the path deformation technique fails because of overlapping branch cuts in complex k_x and k_y planes. Even in periodic structures with period less than a half-wavelength, if a distributed source with a size of more than a half-wavelength is used for excitation, then the spatial period that is considered for the ASM must be a multiple of the structure's actual period to include the entire distributed source. Consequently, the same problem of overlapping branch cuts occurs again, and the path deformation technique cannot be used. All ASM applications reported so far usually use small sources, such as dipole (in 2D periodic structures) or line source (in 1D periodic structures), which always lie only in one unit cell, and the above issue has not before been addressed.

Thus, to compute the scattered field, the path deformation technique is limited only to periodic structures with periods less than a free-space half-wavelength that have been excited with a small source that occupies only one unit cell. It must be mentioned that in Capolino et al. (2007) an example has been given with a period of 0.7λ, but only the currents on strip dipoles have been calculated. It is very important to note that the current, unlike the electric field, has no infinite singularity at branch points; i.e., it does not blow up at branch points, and therefore, as mentioned in Capolino et al. (2007), by careful integration on the real axis, with usual numerical integration rules, the current can be obtained. However, no near electric field result was given therein.

In this article, a new method is introduced that is based on subdividing the original real-axis ASM integration path into segments between the branch points and using the double exponential (DE) quadrature rule for each segment. The DE quadrature rule that was first recommended in Takahasi and Mori (1973) is a powerful numerical quadrature method that can handle integrands with blow-up singularities at end points. It has been

shown by Takahasi and Mori (1973) and Bailey et al. (2005) that the DE quadrature has the best performance among other quadrature rules with the same sampling points.

Another key advantage of this method is its uniform behavior whether the periodic structure contains surface wave poles or not. Because the integration path is subdivided such that SW poles as well as branch points lie at the end points of subintervals, no additional treatment is needed for surface wave (SW) poles.

The remainder of this article is organized as follows. Section 2 describes the ASM briefly and the method of solving the unit cell problem using the IE with the MoM (IE+MoM). The fast evaluation of the periodic Green function (PGF) via the Ewald method is also covered in Section 2.4. In Section 3, the problem of implementation of ASM integration in the presence of overlapping branch cuts is studied, and a new method to extend the ASM for such cases is introduced. This method is based on the DE quadrature rule, which is explained in Section 3.3. In Section 4, the analysis of aperiodic excitation of a free-standing FSS is studied using the suggested method, and some numerical results are given. Finally, Section 5 concludes this work.

2. Statement of the Electromagnetic Problem

In this article, the problem of interest is the interaction between a dipole (aperiodic source) and a 2D periodic structure, as shown in Figure 1. The periodic structure is on a rectangular lattice along x and y with periods of p_x and p_y, respectively. Each unit cell consists of some perfect electric conducting (PEC) objects with arbitrary shapes. The excitation dipole is placed at $\vec{r}_0$ and directed along an arbitrary direction denoted by $\hat{J}$. The time-harmonic dependence $e^{j\omega t}$ is assumed and suppressed throughout. Currently, no commercial electromagnetic software is able to solve the described problem because it has infinite volume and is not periodic.

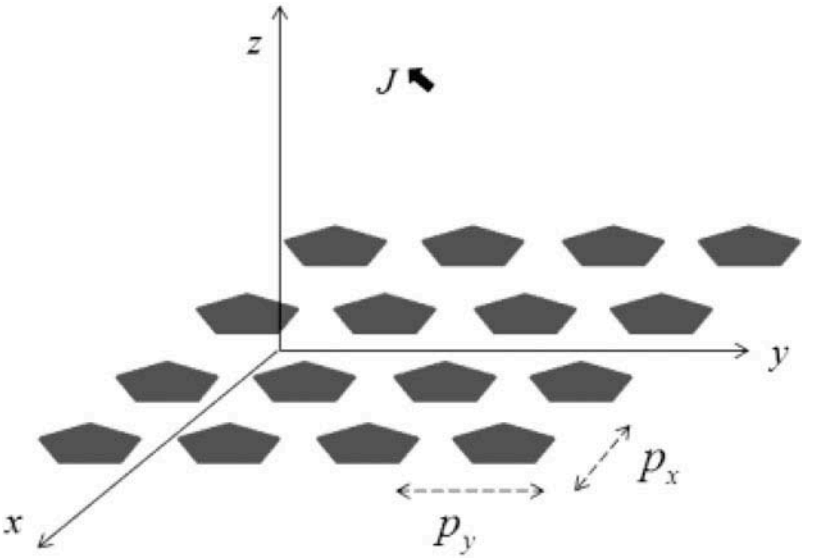

Figure 1. Excitation of FSS by aperiodic dipole source.

2.1. ASM

The ASM is an analytical tool to synthesize the field of an aperiodic source (single source) from a spectral integration of an infinite periodic source (Munk & Burrell, 1979). The basic mathematical relation of the ASM is:

$$\delta(\vec{r}-\vec{r}_0)=\frac{p_x p_y}{(2\pi)^2}\int_{-\pi/p_x}^{\pi/p_x}\int_{-\pi/p_y}^{\pi/p_y}\sum_{m=-\infty}^{\infty}\sum_{n=-\infty}^{\infty}\delta(\vec{r}-\vec{r}_{mn})e^{-jmk_xp_x}e^{-jnk_yp_y}dk_xdk_y, \tag{1}$$

where $\vec{r}$ is the observation point, $\vec{r}_0$ is the location of point source in the (0, 0) unit cell, and $\vec{r}_{mn}=\vec{r}_0+mp_x\hat{x}+np_y\hat{y}$ is the location of the (m, n) source of the phased array. k_x and k_y are impressed phases of the phased array in the x and y directions, respectively. When the integration is performed over the irreducible Brillouin zone $([-\pi/p_x,\pi/p_x]\times[-\pi/p_y,\pi/p_y])$ in Eq. (1), all terms integrate to zero except for $(m,n)=(0,0)$. Using the above identity, the current of a single dipole can be expressed by currents of a 2D periodic phased array of dipoles:

$$\vec{J}^i=\frac{p_x p_y}{(2\pi)^2}\int_{-\pi/p_x}^{\pi/p_x}\int_{-\pi/p_y}^{\pi/p_y}\vec{J}^{i,PA}(k_x,k_y)dk_xdk_y, \tag{2}$$

where $\vec{J}^{i,PA}(k_x,k_y)$ is the current distribution of the infinite phased array of dipoles.

Due to the linearity of source-field relations obtained from Maxwell's equations, the electric field produced by a single dipole $\vec{E}(\vec{r},\vec{r}_0)$ can be expressed by spectral integration of the electric field of the infinite phased array of dipoles $\vec{E}^{PA}(\vec{r},\vec{r}_0,k_x,k_y)$ over the irreducible Brillouin zone:

$$\vec{E}(\vec{r},\vec{r}_0)=\frac{p_x p_y}{(2\pi)^2}\int_{-\pi/p_x}^{\pi/p_x}\int_{-\pi/p_y}^{\pi/p_y}\vec{E}^{PA}(\vec{r},\vec{r}_0,k_x,k_y)dk_xdk_y. \tag{3}$$

Based on Floquet theorem in periodic structures, the electric field of the infinite phase array of dipoles has the following property:

$$\vec{E}^{PA}(\vec{r}+mp_x\hat{x}+np_y\hat{y},\vec{r}_0,k_x,k_y)=\vec{E}^{PA}(\vec{r},\vec{r}_0,k_x,k_y)e^{-jmk_xp_x}e^{-jnk_yp_y}. \tag{4}$$

Hence, the electric field of the original problem in the (m,n) cell can be calculated from the electric field of the infinite phase array in (0, 0) cell:

$$\vec{E}(\vec{r}+mp_x\hat{x}+np_y\hat{y},\vec{r}_0)=\frac{p_x p_y}{(2\pi)^2}\int_{-\pi/p_x}^{\pi/p_x}\int_{-\pi/p_y}^{\pi/p_y}\vec{E}^{PA}(\vec{r},\vec{r}_0,k_x,k_y)e^{-jmk_xp_x-jnk_yp_y}dk_xdk_y. \tag{5}$$

The ASM only involves integration over finite intervals of spectral variables (k_x,k_y) and becomes more efficient than the PWM, which requires infinite integrations. More details about the comparison of the two methods can be found in Capolino et al. (2007).

2.2. IE of Periodic Problem

As explained above, the ASM helps to replace the original problem (aperiodic excitation of a periodic structure) with a spectral integration on the solution of a completely Floquet periodic problem. So the first step to find the solution is to solve the Floquet periodic problem of an infinite phased array radiating next to the periodic structure.

Because of the periodicity, only one unit cell is sufficient to be considered. The solution of the periodic problem is carried out using an electric field IE (EFIE). Usually, by introducing the magnetic vector potential $\vec{A}$ and electric scalar potential V, the EFIE is recast in a mixed potential form, which is preferred because of the lower singularity of its kernel. Let S designate the surface of PEC objects within the unit cell. The following mixed potential integral equation (MPIE) must be solved:

$$-\hat{n}\times\vec{E}^{inc}=\hat{n}\times\left(-j\omega\overleftrightarrow{G}_A*\vec{J}+\frac{1}{j\omega}\nabla\left(G_V*\nabla.\vec{J}\right)\right), \tag{6}$$

where $\vec{E}^{inc}$ is the incident electric field produced by the infinite phased array, $\hat{n}$ is the outside normal to S, $\vec{J}$ is the unknown current density on S, and $\overleftrightarrow{G}_A$ and G_V are the PGFs for the vector and scalar potentials, respectively. Finally $*$ is a shorthand notation of the spatial convolution. The same equations can be written for a magnetic source by defining electric vector potential $\vec{F}$ and magnetic scalar potential W.

2.3. Solution of IE via MoM

Equation (6) can be solved by the MoM. For this purpose, the unknown current density $\vec{J}$ is expanded using well-known first-order Rao-Wilton-Glisson (RWG) basis functions:

$$\vec{J}(\vec{r}\,')=\sum_{n=1}^{N}I_n\vec{f}_n(\vec{r}\,'), \tag{7}$$

where I_n denotes the unknown coefficients, and $\vec{f}_n$ denotes the RWG basis functions that are defined on pairs of triangular subdomains. By substituting Eq. (7) into Eq. (6) and testing the IE by the Galerkin procedure, the following system of linear equations is obtained:

$$[A]_{N\times N}[I]_N=[E]_N, \tag{8}$$

$$\begin{aligned}A_{mn}&=j\omega\mu_0\int_{S_m}\int_{S_n}\vec{f}_m(\vec{r})\cdot\overleftrightarrow{G}_A(\vec{r},\vec{r}\,')\cdot\vec{f}_n(\vec{r}\,')dS'dS\\&\quad+\frac{1}{j\omega\varepsilon_0}\int_{S_m}\nabla.\vec{f}_m(\vec{r})\int_{S_n}G_V(\vec{r},\vec{r}\,')\nabla'.\vec{f}_n(\vec{r}\,')dS'dS,\\E_m&=\int_{S_m}\vec{f}_m(\vec{r})\cdot\vec{E}^{inc}_{\tan}(\vec{r})dS\end{aligned} \tag{9}$$

in which S_m is the domain of the mth testing function, and S_n is the domain of the nth basis function. The above integrals for $m \neq n$ are regular and can be integrated numerically. For $m = n$, the kernel of the MPIE has $1/R$ singularity, which can be extracted and analytically integrated using the formulas in Yla-Oijala and Taskinen (2003) and then added back to the remaining regular part.

2.4. *Evaluation of 2D PGF*

Before solving the MPIE formulation, an accurate and efficient scheme to compute the 2D PGFs $\overleftrightarrow{G}_A$ and G_V is required. For a periodic structure in free space, the dyadic magnetic vector potential is diagonal $\overleftrightarrow{G}_A = \mu_0 G^p \overleftrightarrow{I}$, where $\overleftrightarrow{I}$ is the identity 3 × 3 dyad, while the scalar electric potential is $G_V = G^p/\varepsilon_0$, where G^p is the periodic 2D potential Green function in free space. It is well known that the spatial PGF has a very slow convergence and that some form of acceleration is required (Valerio et al., 2007). The Ewald method, which computes the PGF by splitting it into two fast series with a Gaussian convergent, is proved to be a very powerful method (Valerio et al., 2007). In particular, the Ewald spatial and spectral series for the free-space PGF is

$$\begin{aligned} G^p(\vec{r},\vec{r}\,') &= G^p_{spatial}(\vec{r},\vec{r}\,') + G^p_{spectral}(\vec{r},\vec{r}\,'), \\ G^p_{spec}(\vec{r},\vec{r}\,') &= \frac{1}{4jp_x p_y}\sum_{p=-\infty}^{\infty}\sum_{q=-\infty}^{\infty}\frac{e^{-j\left(k_{xp}(x-x')+k_{yq}(y-y')\right)}}{k_{z,pq}}\cdot \\ &\qquad \sum_{\pm} e^{\pm jk_{z,pq}(z-z')}\operatorname{erfc}\left(\frac{jk_{z,pq}}{2E}\pm(z-z')E\right), \\ G^p_{spat}(\vec{r},\vec{r}\,') &= \frac{1}{4\pi}\sum_{m=-\infty}^{\infty}\sum_{n=-\infty}^{\infty}\frac{e^{-j(mk_x p_x+nk_y p_y)}}{R_{mn}}\cdot\sum_{\pm} e^{\pm jk_0 R_{mn}}\operatorname{erfc}\left(\frac{jk_0}{2E}\pm R_{mn}E\right); \end{aligned} \tag{10}$$

in the above equations, $R_{mn} = \left|\vec{r} - \vec{r}\,' - mp_x\hat{x} - np_y\hat{y}\right|$ is the distance between observation point $\vec{r}$ and the source in the (m,n) unit cell. k_0 is the free-space wavenumber, and

$$k_{xp} = k_x + \frac{2\pi p}{p_x}, \quad k_{yq} = k_y + \frac{2\pi q}{p_y}, \quad k_{z,pq} = \sqrt{k_0^2 - k_{xp}^2 - k_{yq}^2}, \tag{11}$$

where $\operatorname{erfc}(w)$ is the complementary error function, which can be evaluated through different methods (Weideman, 1994). The splitting parameter E has a major influence in convergence of the two series. The details of choosing the best value for E was studied in Celepcikay et al. (2008). It must be noted that in the IE solution or field computation, the gradient or curl of 2D PGFs may be needed. Because of the uniform convergence of the Ewald spatial and spectral series, the curl and gradient of 2D PGFs can be obtained from direct term-by-term differentiation of Eq. (10).

3. Implementation Problems

In numerical implementation of the above-mentioned procedure to solve the described electromagnetic problem, the most important and sensitive step is the ASM spectral

integration in Eq. (3). The integration path lies on the real axes of complex k_x and k_y planes on which the integrand $\vec{E}^{PA}(\vec{r},\vec{r}_0,k_x,k_y)$ has an infinite number of branch points that are the result of $1/k_{z,pq}$ in Eq. (10). However, depending on the period-to-wavelength ratio, only a limited number of these branch points lie inside the integration interval in both planes. These branch points are obtained from $k_{xp}^2+k_{yq}^2=k_0^2$. For a fixed k_y, the branch points in the k_x plane are

$$k_{xb}^{p,q}=\pm\sqrt{k_0^2-k_{yq}^2}+\frac{2\pi p}{p_x}. \tag{12}$$

Moreover, in Lovat et al. (2011), it was shown that the branch points in the k_y plane are

$$k_{yb}^{q}=\pm k_0+\frac{2\pi q}{p_y}. \tag{13}$$

Therefore, the number of branch points lying in the interval $-\pi/p_i \le k_i \le \pi/p_i$, $(i=x,y)$ depends on the corresponding period to wavelength ratio. To compute the spectral integral in Eq. (3) accurately, the position of branch points becomes important, and suitable schemes must be considered.

3.1. Case 1: Short Periods (below Half-Wavelength)

If $p_x,p_y<\lambda_0/2$, exactly one pair of branch points lies within the integration intervals in the k_x and k_y complex planes. Specifically, branch points in the k_x and k_y planes occur at $k_{x,b}=\pm\sqrt{k_0^2-k_y^2}$ and $k_{y,b}=\pm k_0$, respectively, which are inside intervals $-\pi/p_x \le k_x \le \pi/p_x$ and $-\pi/p_y \le k_y \le \pi/p_y$. In this case, as shown in Figure 2, a suitable path deformation avoids crossing the branch points and branch cuts while staying on the top Riemann sheet (the sheet in which the imaginary part of $k_{z,pq}$ is negative) in the k_y plane. Different path deformations can be selected (Lovat et al., 2011). The positions of the branch points and their corresponding Sommerfeld branch cuts in the k_x plane show that the same deformed path can also be chosen in the k_x plane.

3.2. Case 2: Long Periods (above Half-Wavelength)

In this case, depending on the ratio of period to wavelength, the branch cuts of adjacent branch points overlap for both the k_x and k_y planes. Without loss of generality, it is assumed that $\lambda_0/2<p_x,p_y<\lambda_0$. For this assumption, exactly two pairs of branch cuts overlap within the original integration path. As shown in Figure 3, because of long periods, the branch cuts in the k_y plane completely surround the beginning and end points of the integration interval. The same problem occurs in the k_x plane for each value of k_y. Hence, every deformation in the path of integration crosses the branch cuts, and the path goes to an improper Riemann sheet, which causes the ASM integration to fail. Therefore, path deformation is not applicable for structures with periods larger than a half-wavelength.

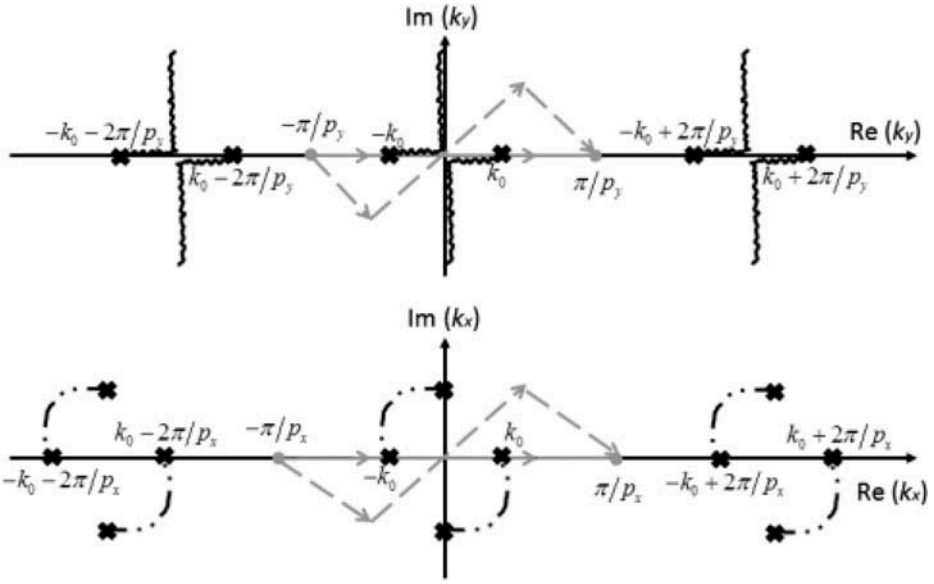

Figure 2. Original (solid gray line) and deformed (dashed gray line) integration paths in both complex planes. Branch points are indicated with crosses, and the Sommerfeld branch cuts are also shown. The movement of branch points in the k_x plane while moving on the path of integration in the k_y plane is shown with a black dash–dot line.

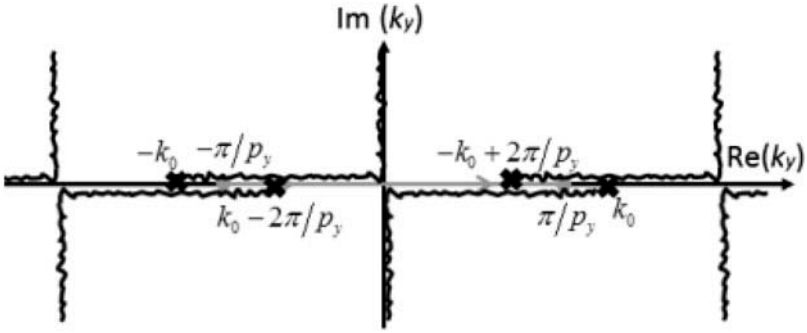

Figure 3. Overlapping branch cuts surround parts of the integration intervals in the k_y plane, and every path deformation crosses the branch cut and goes to improper Riemann sheet.

In particular, to compute the scattered field of the periodic structure excited by an aperiodic source, one must compute the ASM integration of

$$\vec{E}^{sca}(k_x,k_y,\vec{r}) = \frac{1}{j\omega\varepsilon}\sum_{n=1}^{N} I_n(k_x,k_y).\left(k^2\int_{f_n} G(k_x,k_y,\vec{r},\vec{r}\,')\vec{f}_n(\vec{r}\,')ds' + \nabla\int_{f_n} G(k_x,k_y,\vec{r},\vec{r}\,')\nabla.\vec{f}_n(\vec{r}\,')ds'\right), \tag{14}$$

in which G is the PGF of the structure, and $I_n, \vec{f}_n$ are the same as in Eq. (7). Since $I_n(k_x, k_y)$ is the solution of matrix equation (Eq. (8)) and every element of the impedance matrix has all the above-mentioned overlapping branch cuts, every path deformation crosses the branch cuts, and ASM integration will fail.

After an extensive review of literature, it seems that so far, every result based on the ASM is given for structures with short periods (Araneo et al., 2011; Lovat et al., 2011; Capolino et al., 2005a, 2005b; Rodriguez-Berral et al., 2009; Yang, 1999, 2001, 2004) except for Capolino et al. (2007). However, Capolino et al. (2007) only obtained the current distribution of an array of strip dipoles excited by an electric dipole with a period-to-wavelength ratio of 0.7. However, as mentioned before, the current, unlike the electric field, has no blow-up singularity at branch points because when a branch point is approached in the complex k_x (or k_y) plane, the matrix elements (A_{mn}, E_m) of Eq. (9) have the same singular behavior so that the limit of Eq. (8) at a branch point gives finite values for currents. Consequently, currents can be obtained by using a conventional numerical quadrature on real axis without any path deformation (Capolino et al., 2007). However, no near field was calculated in that study because the PGF G, which appears in Eq. (14), introduces blow-up singularities at branch points.

In the proposed method, the original integration intervals in both the k_x and k_y planes are divided into some subintervals such that the integrand has no singularity in each subinterval except at the end points. Then the ASM integration is performed using the DE quadrature rule, explained in the next section.

Let the reader focus on a particular case when $\lambda_0/2 < p_x, p_y < \lambda_0$. The method is general, and it is easy to modify it for larger periods. When $\lambda_0/2 < p_y < \lambda_0$, exactly two singular branch points lie in the main integration interval at $-k_0 + 2\pi/p_y$ and $k_0 - 2\pi/p_y$, as shown in Figure 3. To perform the integration, the main interval $(-\pi/p_y, \pi/p_y)$ is divided into three subintervals as follows:

$$S^1_{k_y} : \left(\frac{-\pi}{p_y}, k_0 - \frac{2\pi}{p_y}\right), \quad S^2_{k_y} : \left(k_0 - \frac{2\pi}{p_y}, -k_0 + \frac{2\pi}{p_y}\right), \quad S^3_{k_y} : \left(-k_0 + \frac{2\pi}{p_y}, \frac{\pi}{p_y}\right). \tag{15}$$

The integrand of ASM integration in Eq. (3) is analytic on these subintervals except at one or both end points. This is an important condition for the DE quadrature rule.

For the k_x plane, the branch cuts are more sophisticated, because changing the value of k_y from Eq. (15) will result in a change of the position of branch points and branch cuts in the k_x plane. As an example, assume $p_x = p_y = 0.75\lambda$ or, equivalently, $k_0 = 1.5\pi/p_y$. The branch cuts in the k_x plane for $k_y = -0.55\pi/p_y$ are shown in Figure 4(a). Note that four singular branch points lie inside the integration interval ($k^{0,1}_{xb}, -k^{0,1}_{xb}, k^{1,0}_{xb}, -k^{-1,0}_{xb}$). The first and second branch points are due to the term $(p, q) = (0, 1)$ in the Ewald spectral summation in Eq. (10). The third and fourth branch points, respectively, are due to the terms $(p, q) = (1, 0)$ and $(p, q) = (-1, 0)$ in Eq. (10). Hence, to perform DE integration on the main interval of the k_x plane for this value of k_y, the interval $(-\pi/p_x, \pi/p_x)$ must be divided into the following five subintervals:

$$\begin{gathered} S^1_{k_x} : \left(-\pi/p_x, k^{1,0}_{xb}\right), \quad S^2_{k_x} : \left(k^{1,0}_{xb}, -k^{0,1}_{xb}\right), \quad S^3_{k_x} : \left(-k^{0,1}_{xb}, k^{0,1}_{xb}\right), \\ S^4_{k_x} : \left(k^{0,1}_{xb}, -k^{-1,0}_{xb}\right), \quad S^5_{k_x} : \left(-k^{-1,0}_{xb}, \pi/p_x\right). \end{gathered} \tag{16}$$

Now, if the value of k_y changes to $-0.35\pi/p_y$, the branch points positions and the branch cuts in the k_x plane change, and the singular branch points $k^{0,1}_{xb}, -k^{0,1}_{xb}$ move from the

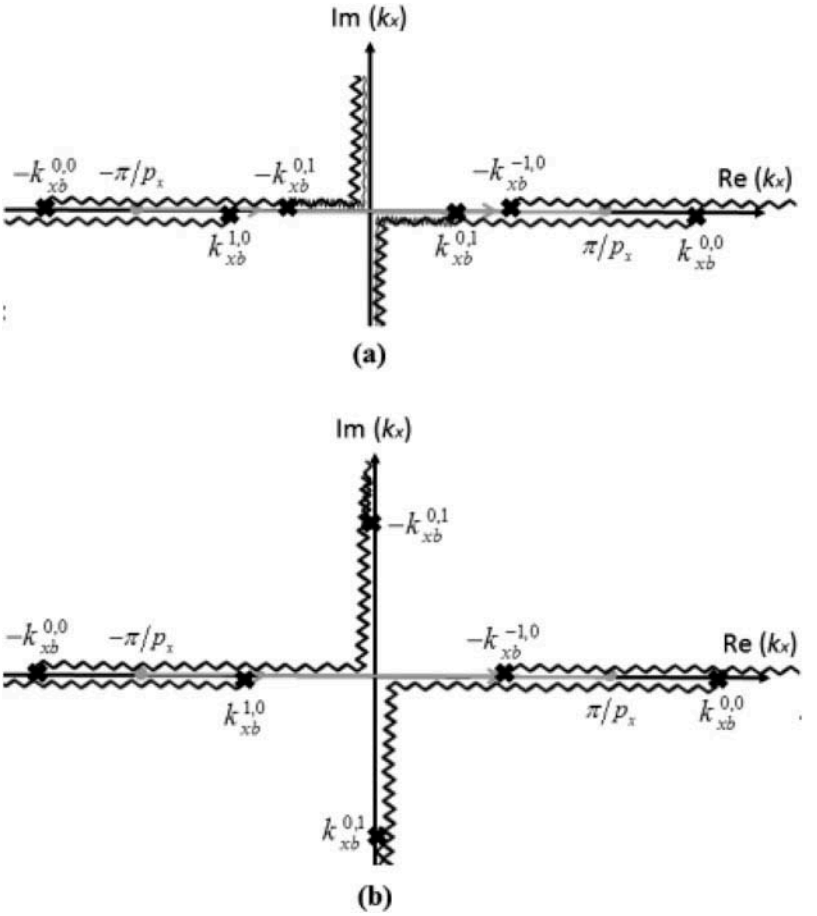

Figure 4. Branch points and Sommerfeld branch cuts in the k_x plane for: (a) $k_y = -0.55\,\pi/p_y$ and (b) $k_y = -0.35\,\pi/p_y$.

integration interval onto the imaginary axis, as shown in Figure 4(b). Hence, for the value of $k_y = -0.35\,\pi/p_y$, it is enough to divide the k_x interval into three subintervals:

$$S_{k_x}^1 : \left(\frac{-\pi}{p_x}, k_{xb}^{1,0}\right), \quad S_{k_x}^2 : \left(k_{xb}^{1,0}, -k_{xb}^{-1,0}\right), \quad S_{k_x}^3 : \left(-k_{xb}^{-1,0}, \frac{\pi}{p_x}\right). \tag{17}$$

The above example shows that in numerical implementation of the ASM using the DE quadrature, the key point is to extract the singular branch points of the k_x plane that lay inside the original integration interval $(-\pi/p_x, \pi/p_x)$. This must be done repeatedly after every change of k_y value, which is assumed to be the first integration variable of the ASM. After proper subdivision of the integration path, the DE quadrature rule can be employed to evaluate the ASM integral in each segment.

3.3. DE Quadrature Rule

The DE quadrature rule (DE formula) was introduced by Takahasi and Mori (1973). The DE formula is a general, robust, and very efficient numerical integration method. This method, unlike standard quadrature rules, such as the midpoint or Gaussian methods, can handle integrands with blow-up singularities at the end points of the integration interval. Consider the following integral:

$$I = \int_{-1}^{+1} f(x)\, dx. \tag{18}$$

With variable transformation of $x = \varphi(t) = \tanh\left(\frac{\pi}{2}\sinh(t)\right)$, the above integral changes to

$$I = \int_{-\infty}^{+\infty} f(\varphi(t))\varphi'(t)dt, \tag{19}$$

in which

$$\varphi'(t) = \frac{\frac{\pi}{2}\cosh(t)}{\cosh^2\left(\frac{\pi}{2}\sinh(t)\right)} \approx O\left(\exp\left(\frac{-\pi}{2}\exp(|t|)\right)\right), \tag{20}$$

as $|t| \to +\infty$. Discretization of the above integral using the trapezoidal rule gives

$$I_N = h\sum_{m=-n}^{n} f(\varphi(mh))\varphi'(mh), \tag{21}$$

where $N = 2n + 1$ is the number of function samples. In Takahasi and Mori (1973), it was proved that for numerical integration of an analytic function over $(-\infty, +\infty)$, the uniform trapezoidal rule is optimal among formulas with the same sampling points. Takahasi and Mori (1973) also showed that the above variable transformation, which is called tanh–sinh transformation, is an optimal transformation from the error viewpoint. It means that Eq. (21) with tanh–sinh transformation gives the best approximation for the integral of Eq. (18) among different variable transformations. The DE quadrature rule is due to DE decay of Eq. (20). It was shown in Takahasi and Mori (1973) that the DE quadrature has faster decay than other quadrature rules.

The most important feature of the DE quadrature is its ability to handle the end-point blow-up singularities. It can handle different types of singularities, such as branch points and poles. DE formulation can approach the end-point singularity as closely as desired, while its very fast decaying weights cancel the fast growing function samples. It must be noted that in DE formulation, the integrand must be analytic everywhere except at the end points. The comparison of DE quadrature rule with other powerful quadrature formulas can be found in Takahasi and Mori (1973) and Bailey et al. (2005).

It is worth noticing that the DE formulation suffers from two problems that can occur due to careless computer implementation (Bailey et al., 2005). First is the loss of significant digits due to singularities of the $(1 \pm x)^{-1+\delta}$ type, where δ is a small positive constant. The second is the overflow due to the denominator of Eq. (20). The methods to

overcome these problems and more details about DE quadrature can be found in Takahasi and Mori (1973) and Bailey et al. (2005).

4. Numerical Results

In this section, some numerical results are presented to illustrate the application of the proposed implementation of the ASM. Since, the near field of structures with periods larger than a half-wavelength have not been studied in the literature, the focus here is only on these structures.

4.1. *Single Dipole in Free Space*

As the first example, the electric field of a single dipole is obtained by using the ASM integration of a phased array of dipoles with periods larger than a half-wavelength. Because this example does not involve any PEC object, no IE and MoM are required. This example serves to verify the method described in Section 3.2 using the analytic expression of the electric field of a single dipole, which is given by

$$\vec{E}_{dipole} = -j\omega\mu_0 \frac{e^{-jk_0R}}{4\pi R}\vec{I}\cdot\hat{J} - \frac{j}{\omega\varepsilon_0}\left(\nabla\nabla\frac{e^{-jk_0R}}{4\pi R}\right)\cdot\hat{J}. \tag{22}$$

Figure 5 shows the electric field amplitude of the dipole obtained by the ASM at two different frequencies (f = 1.7 GHz). For each frequency, the electric field is calculated using two different values of period-to-wavelength ratio $\left(p_{x,y}/\lambda = 0.6, 0.8\right)$. The dipole is y-directed and placed at the origin while the observation point is at (3 cm, 2 cm, z cm). Excellent agreement between the ASM values with exact values can be seen in Figure 5.

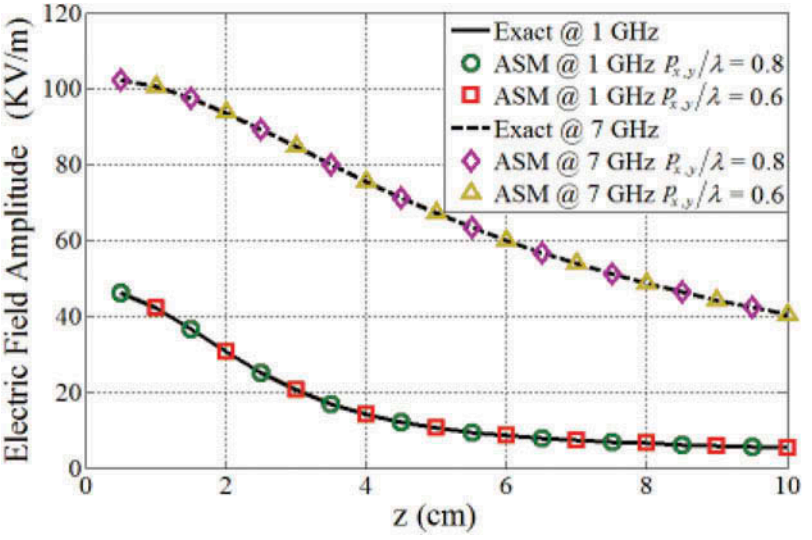

Figure 5. Electric field amplitude of single dipole in free space obtained via the ASM and the exact analytic formula.

4.2. Single Dipole in Front of a Free-Standing FSS

The second example consists of a free-standing FSS that is excited by a single electric dipole. The FSS unit cell consists of a rectangular PEC patch that is centered at origin. The width and length of each patch are w = 5.08 mm and l = 25.4 mm, as shown in Figure 6. Spatial periods of the structure are p_x = 35.6 mm and p_y = 35.6 mm in the x and y directions, respectively. The structure is on the $z = 0$ plane, and a horizontal electric dipole at $(0, 0, z_s)$ excites the FSS. The parameters of interest are the reflection and transmission coefficients, which are defined, respectively, by $R(r) = \left|E^{sca}_{tot}(r)\right| / \left|E^{inc}_{tot}(r)\right|$ and $T(r) = \left|E^{tra}_{tot}(r)\right| / \left|E^{inc}_{tot}(r)\right|$.

This problem cannot be solved by commercial electromagnetic (EM) simulators because of its infinite size and nonperiodic nature. However, for the sake of comparison, a large but finite structure was simulated using FEKO (EM Software & Systems). The simulated structure includes 31 × 31 FSS unit cells. This size was obtained experimentally to have an acceptable truncation error in the results. Each PEC patch is divided into 34 triangles, both in FEKO and in the proposed method. Reflection and transmission coefficients of the FSS for three different values of electric dipole positions are shown in Figures 7 and 8, respectively.

The observation point for reflection calculations is at (0, 0, 7 cm), while it is assumed to be (0, 0, –7 cm) for transmission calculations. Such an analysis was performed by Lovat et al. (2011) for a strip-mesh screen and an array of PEC spheres, but the ratio of period to wavelength for these structures was 0.2 and 0.33, respectively. In this FSS for frequencies above 4.21 GHz, the period is larger than a half-wavelength. As can be seen, the ASM results are in excellent agreement with those of FEKO, while the ASM method is six times faster than the simulation in FEKO for the same number of frequencies and the same meshing. Figures 7 and 8 also show that the reflection and transmission coefficients in the

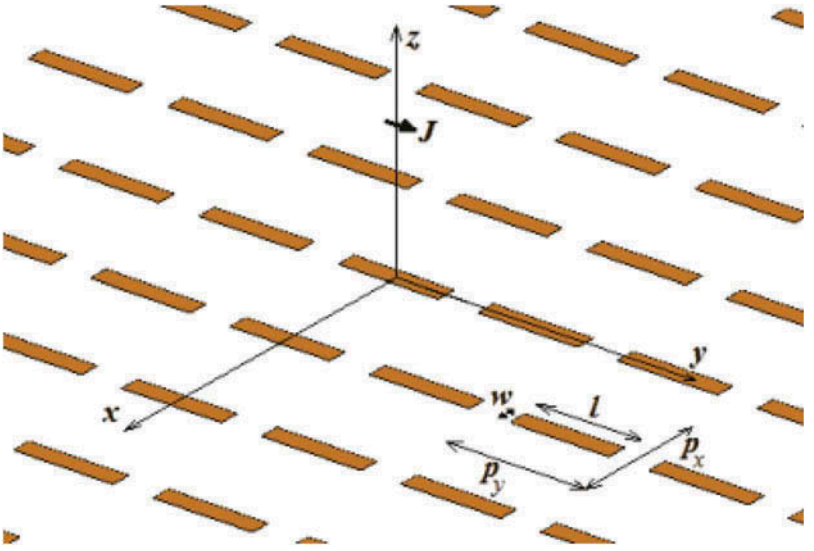

Figure 6. Free-standing FSS excited by a single electric dipole.

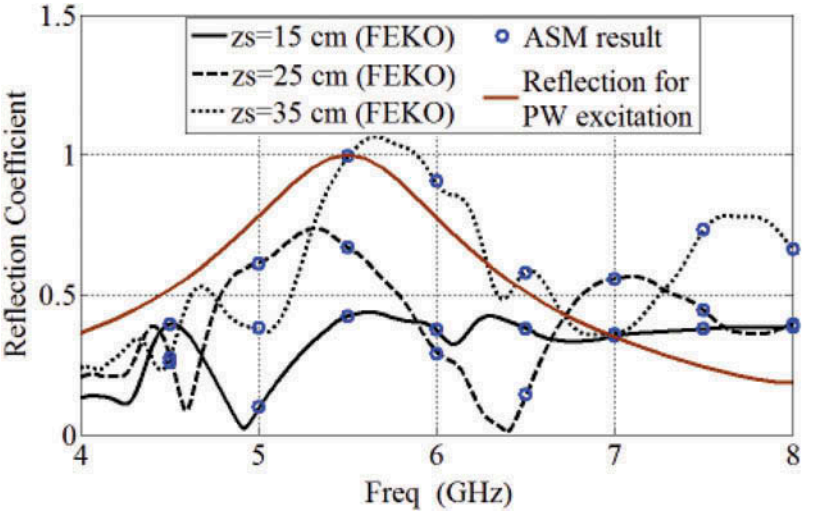

Figure 7. Reflection coefficient of free-standing FSS for different values of z_s.

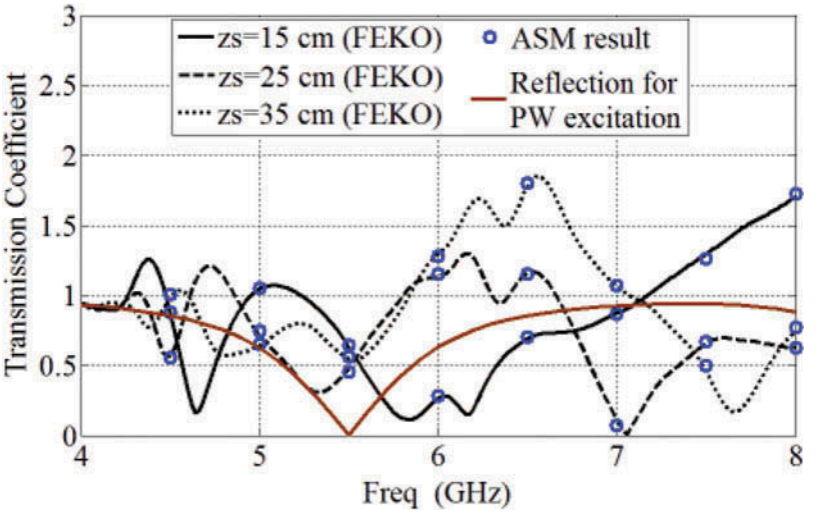

Figure 8. Transmission coefficient of free-standing FSS for different values of z_s.

planewave excitation of FSS are very different from the excitation of structure with a finite source.

To demonstrate the ability of this method, the near field of the FSS has been calculated at $f = 6$ GHz with the dipole positioned at $z_s = 25$ cm. The total electric field in three azimuthal planes for different values of ρ (radial distance from the z-axis) was calculated, and the results are shown in Figure 9 with those obtained from FEKO. The observation plane is at $z = 7$ cm. Finally, individual components of the total electric field obtained from the ASM have been shown in Figure 10.

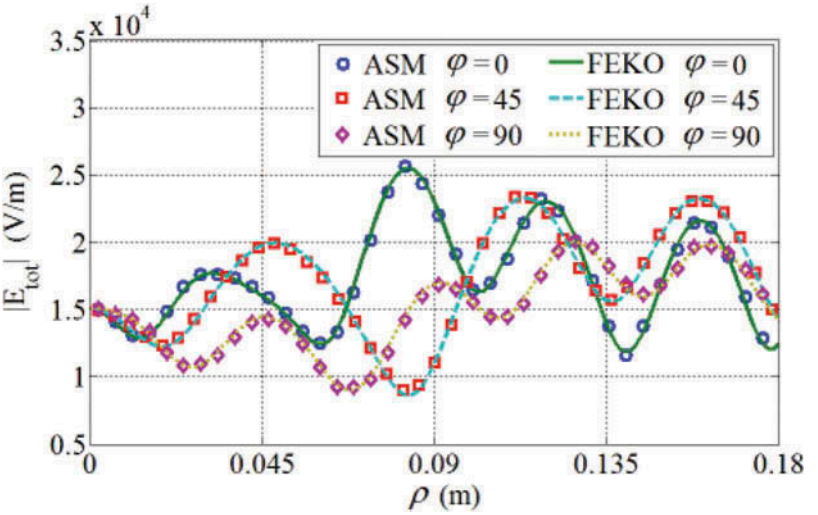

Figure 9. Magnitude of total electric field in z = 7 cm and φ = 0°, 45°, and 90° at f = 6 GHz. The electric dipole source is z_s = 25 cm. ASM results have been specified with marks on FEKO results.

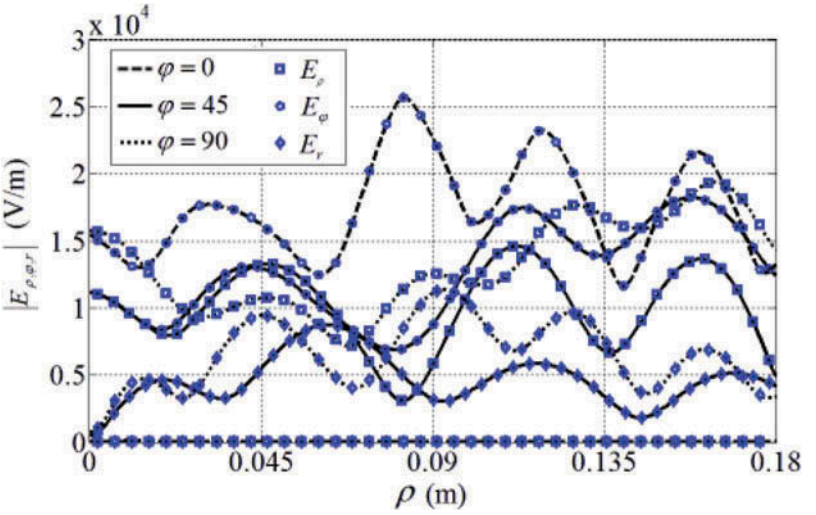

Figure 10. Magnitude of components of electric fields (parameters are the same as in Figure 9). All curves have been calculated with the ASM method.

5. Conclusion

Aperiodic excitation of periodic structures for different values of period-to-wavelength ratio was thoroughly revisited. It has been shown that in the case of a small period, the ASM can be applied with path deformation technique because the suitable path (the path that is completely on the top Riemann sheet) can be found easily. This method has been used in the literature, but it was shown that when the period is larger than a half-wavelength, the branch cuts overlap, and path deformation is not applicable.

To alleviate this problem and apply the ASM to structures with large periods, a new method was proposed. This method is based on proper subdivision of original integration intervals and using the DE quadrature integration. DE formulation has been proved as the most efficient rule for blow-up singularity of integrands at the end points of the interval. The numerical results of the electric field and reflection and transmission coefficients of a free-standing FSS excited by an electric dipole were compared to those obtained from FEKO with perfect agreement.

References

Araneo, R., G. Lovat, & S. Celozzi. 2011. Shielding effectiveness of periodic screens against finite high-impedance near-field sources. *IEEE Trans. Electromag. Compat*. 53:706–716.

Bailey, D. H., K. Jeyabalan, & X. S. Li. 2005. A comparison of three high-precision quadrature schemes. *Exp. Math*. 14:317–329.

Capolino, F., D. R. Jackson, & D. R. Wilton. 2005a. Fundamental properties of the field at the interface between air and a periodic artificial material excited by a line source. *IEEE Trans. Antennas Propagat*. 53:91–99.

Capolino, F., D. R. Jackson, & D. R. Wilton. 2005b. Mode excitation from sources in two-dimensional EBG waveguides using the array scanning method. *IEEE Trans. Microw. Wirel. Comp. Lett*. 15:49–51.

Capolino, F., D. R. Jackson, D. R. Wilton, & L. B. Felsen. 2007. Comparison of methods for calculating the field excited by a dipole near a 2D periodic material. *IEEE Trans. Antennas Propagat*. 55:1644–1655.

Celepcikay, F. T., D. R. Wilton, D. R. Jackson, & F. Capolino. 2008. Choosing splitting parameters and summation limits in the numerical evaluation of 1D and 2D periodic Green's functions using the Ewald method. *Radio Sci*. 43(6):1–11.

Lee, Y. J., J. Yeo, R. Mittra, & W. S. Park. 2005. Application of electromagnetic bandgap (EBG) superstrates with controllable defects for a class of patch antennas as spatial angular filters. *IEEE Trans. Antennas Propagat*. 53:224–235.

Llombart, N., A. Neto, G. Gerini, & P. de Maagt. 2005. Planar circularly symmetric EBG structures for reducing surface waves in printed antennas. *IEEE Trans. Antennas Propagat*. 53:3210–3218.

Lovat, G., R. Araneo, & S. Celozzi. 2011. Dipole excitation of periodic metallic structures. *IEEE Trans. Antennas Propagat*. 59:2178–2187.

Munk, B., & G. Burrell. 1979. Plane-wave expansion for arrays of arbitrarily oriented piecewise linear elements and its application in determining the impedance of a single linear antenna in a lossy half-space. *IEEE Trans. Antennas Propagat*. 27:331–343.

Rodriguez-Berral, R., F. Mesa, P. Baccarelli, & P. Burghignoli. 2009. Excitation of a periodic microstrip line by an aperiodic delta-gap source. *IEEE Antennas Wireless Propagat. Lett*. 8:641–644.

Takahasi, H., & M. Mori. 1973. Double exponential formulas for numerical integration. *Publicat. Res. Inst. Math. Sci*. 9:721–741.

Valerio, G., P. Baccarelli, P. Burghignoli, & A. Galli. 2007. Comparative analysis of acceleration techniques for 2-D and 3-D Green's functions in periodic structures along one and two directions. *IEEE Trans. Antennas Propagat*. 55:1630–1643.

Weideman, J. A. C. 1994. Computation of the complex error function. *SIAM J. Numer. Anal*. 31:1497–1518.

Yang, F., & Y. Rahmat-Samii. 2009. *Electromagnetic band gap structures in antenna engineering*. New York. MA: Cambridge University Press, Chapter 2.

Yang, H. Y. D. 1999. Theory of antenna radiation from photonic band-gap materials. *Electromagnetics* 19:255–276.

Yang, H. Y. D. 2001. Surface waves of printed antennas on planar artificial periodic dielectric structures. *IEEE Trans. Antennas Propagat*. 49:444–450.

Yang, H. Y. D. 2004. Analysis of microstrip dipoles on planar artificial periodic dielectric structures. *J. Electromag. Waves Appl*. 18:1373–1388.

Yla-Oijala, P., & M. Taskinen. 2003. Calculation of CFIE impedance matrix elements with RWG and $n \times$ RWG functions. *IEEE Trans. Antennas Propagat*. 51:1837–1846.

Zhao, T., D. R. Jackson, J. T. Williams, H. Y. D. Yang, & A. A. Oliner. 2005. 2D periodic leaky-wave antennas—Part I: Metal patch design. *IEEE Trans. Antennas Propagat*. 53:3505–3514.